nature climate change

SUPPLEMENTARY INFORMATION

DOI: 10.1038/NCLIMATE

Changes in large-scale climate alter spatial synchrony of aphid pests

Lawrence W Sheppard, James R. Bell, Richard Harrington & Daniel C Reuman

1 Supplementary figures

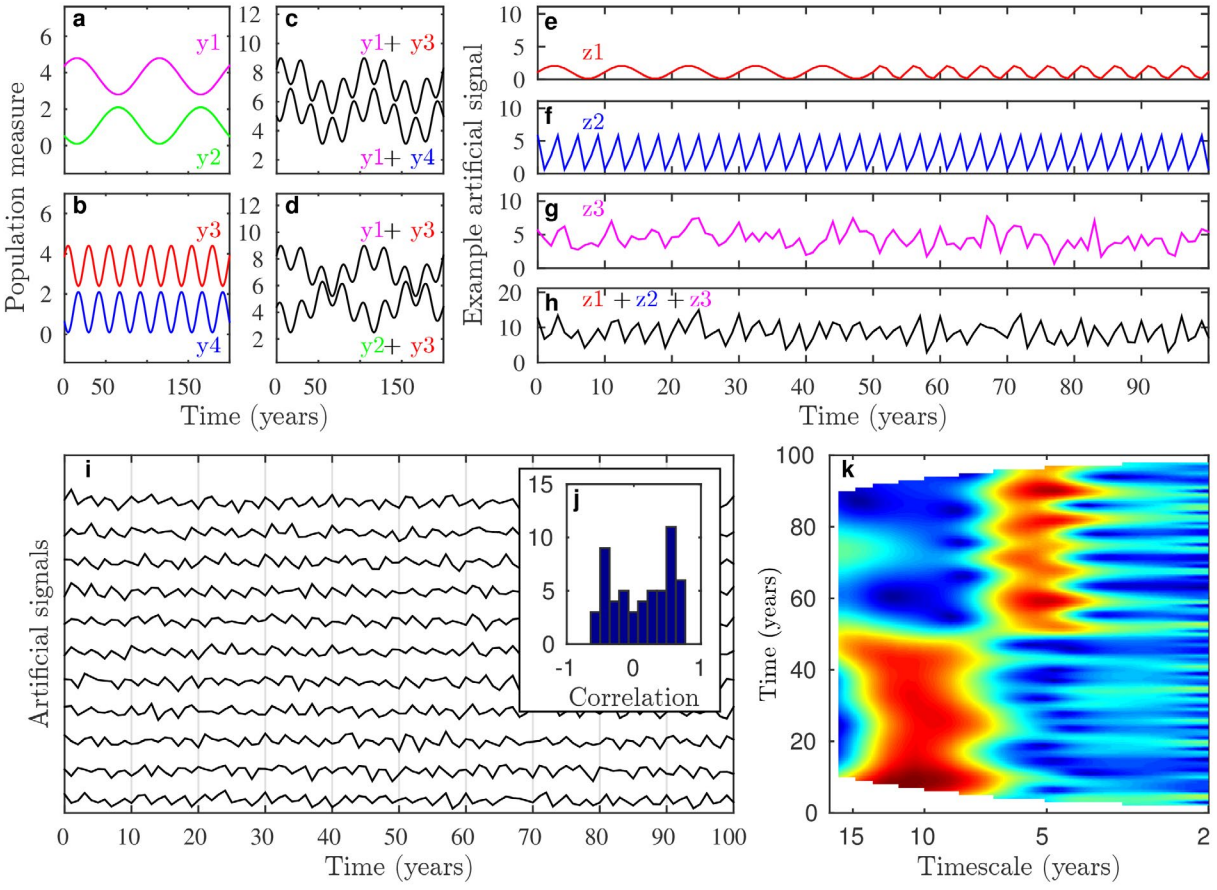

Supplementary Figure 1. Detecting time- and timescale-specific synchrony with the wavelet mean field. Panels a-d show the principle of how synchrony can differ for different timescales of dynamics. Time series y1 and y2 (a) are exactly anti-correlated (out of phase), as are y3 and y4 (b). Combining y1 with y3 and y1 with y4 gives two time series (c) which are synchronized on long timescales, but anti-synchronized on short timescales. The reverse is also possible (d). This timescale-specific structure of synchrony cannot be detected with correlation coefficients, which are 0 for both c and d, because contributions from different timescales cancel. In practice, real population and environmental signals are broadband, and exact cancellation is unlikely, but asynchrony at some frequencies can strongly conceal important synchrony at other frequencies. Panels e-k demonstrate this concealment, using artificial data, and also show how the wavelet mean field detects time- and timescale-specific synchrony. Each of 11 artificial time series were constructed as the sum of: 1) a single common signal of amplitude 1 that changes its oscillatory period at $t = 50$ from 10 years to 5 years (e); 2) oscillations of amplitude 3 that have the same oscillatory period (3

years), but random and independent phases in each of the 11 constructed time series (f); and 3) white noise of standard deviation 1.5, again independently generated for each of the 11 time series (g). Synchrony in the resulting time series cannot be visually detected (i), nor is it readily apparent by examining the 55 pairwise correlation coefficients between time series (j), which spanned a wide range of values including 0. But the wavelet mean field magnitude (k) showed clear colour bands at 10-year period for $t < 50$ and 5-year period for $t > 50$. The wavelet mean field magnitude displays strength of synchrony as a function of timescale of dynamics and time, here with red indicating synchrony and blue asynchrony. Definition and details of wavelet mean fields are in Methods.

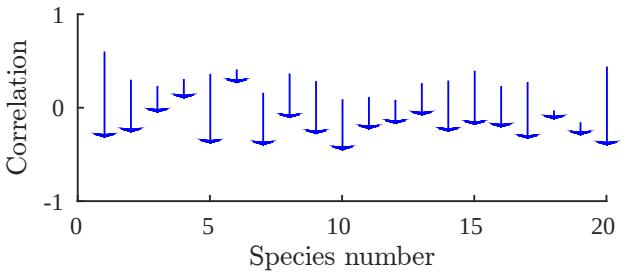

Supplementary Figure 2. Lag-1 autocorrelation statistics for species-averaged first flight time series. For the periods before (arrow tails) and after (arrow heads) 1993. Correlations decreased, corresponding to decreased year-to-year consistency and increased volatility of average first flight times.

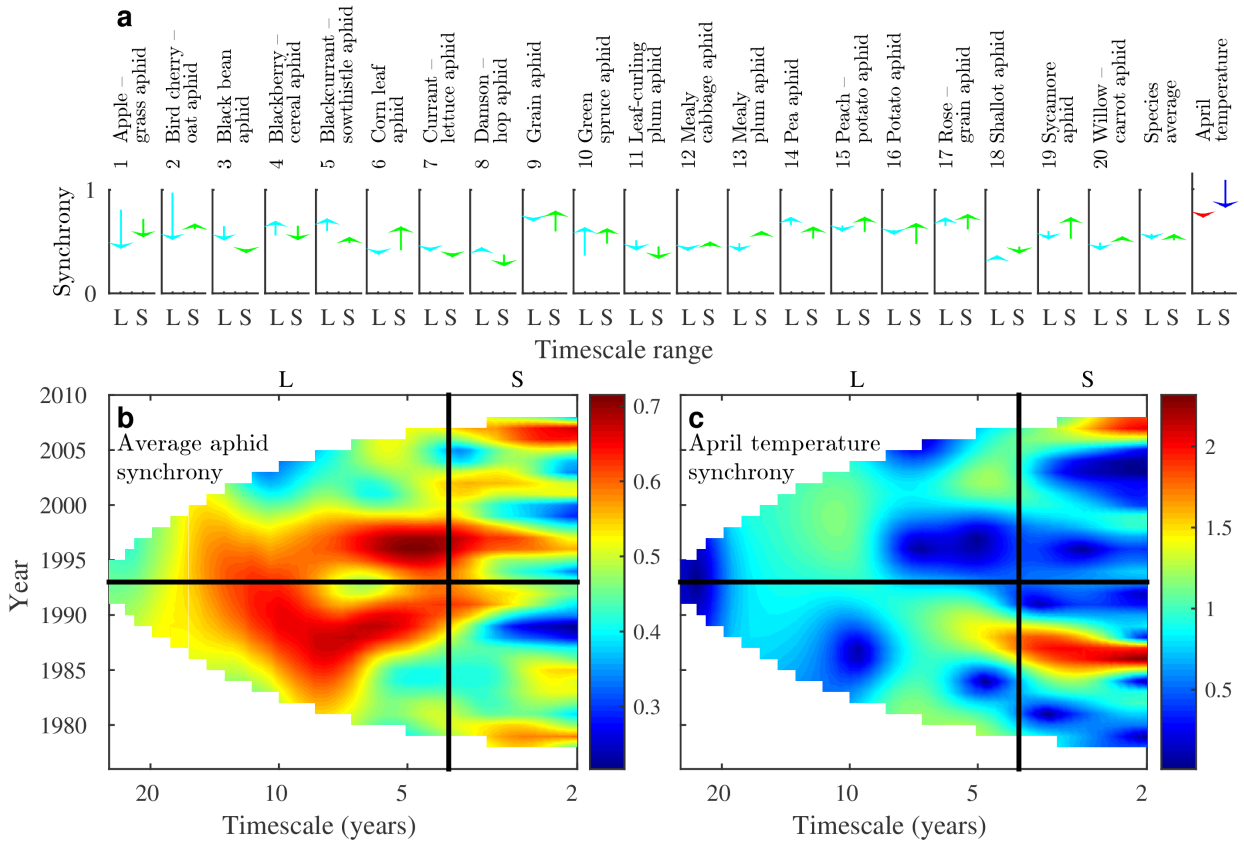

Supplementary Figure 3. Synchrony in flight duration, and in April temperature. Same format as Fig. 1, but small panels (a) show changes in the synchrony of flight duration and April temperature time series, and colour surface plots are wavelet mean field magnitudes showing synchrony on average across species for flight duration (b) and for April temperatures (c). Flight duration time series were reasonably well synchronized across sites, and often showed timescale structure of synchrony and changes in synchrony through time (a), but time- and timescale-specific patterns of synchrony differed between species, so the average colour surface plot (b) shows predominantly low values compared to Fig. 1b. Patterns of April temperature synchrony (c) did not resemble average patterns of synchrony across species for first flight (Fig. 1b), flight duration (this figure, b) or total aphid count (Supplementary Fig. 4b).

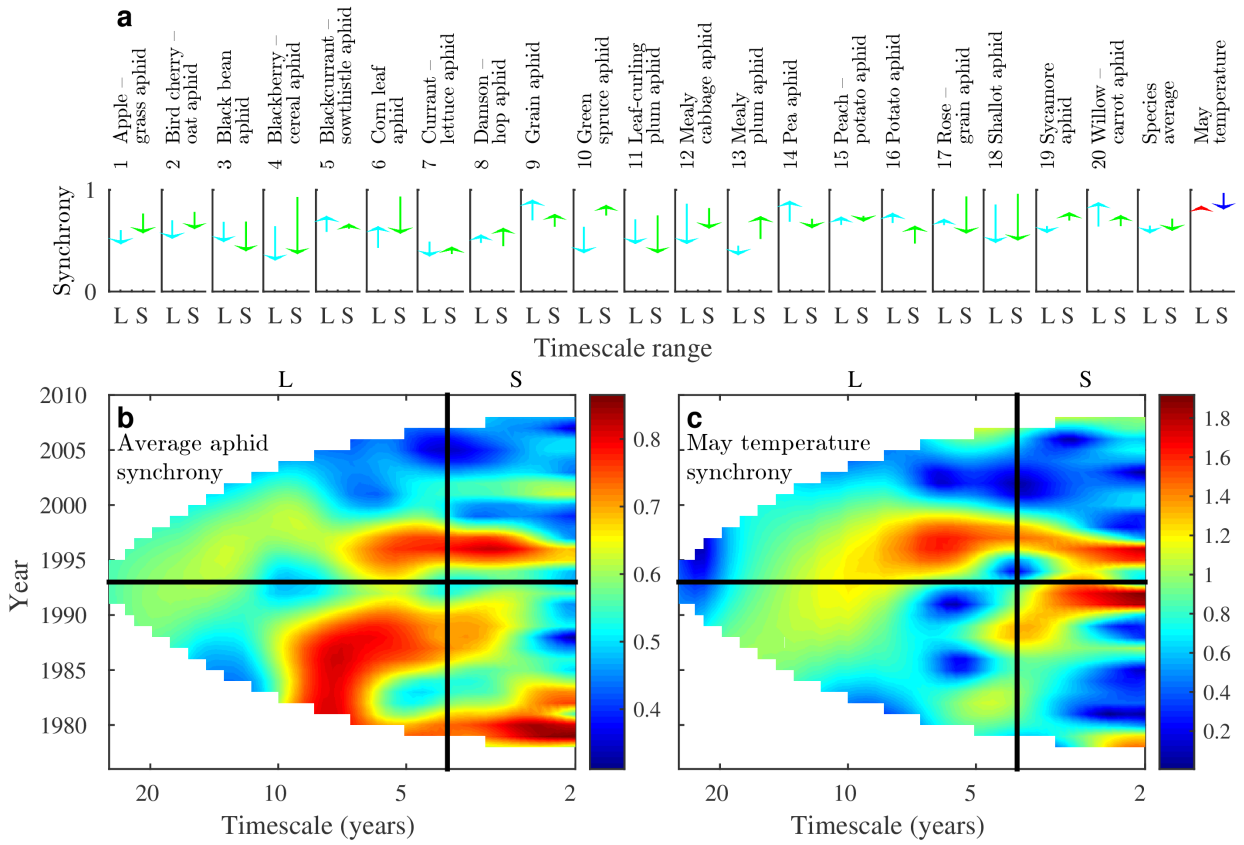

Supplementary Figure 4. Synchrony in total aphid counts, and in May temperature. Same format as Fig. 1, but small panels (a) show changes in the synchrony of total aphid counts and May temperature time series, and colour surface plots are wavelet mean field magnitudes showing synchrony on average across species for count (b) and for May temperatures (c). Total aphid count time series were reasonably well synchronized across sites, and often showed timescale structure of synchrony and changes in synchrony through time (a), but time- and timescale-specific patterns of synchrony differed between species, so the average colour surface plot (b) shows predominantly low values compared to Fig. 1b. Patterns of May temperature synchrony (c) did not resemble average patterns of synchrony across species for first flight (Fig. 1b), flight duration (Supplementary Fig. 3b) or total aphid count (this figure, b).

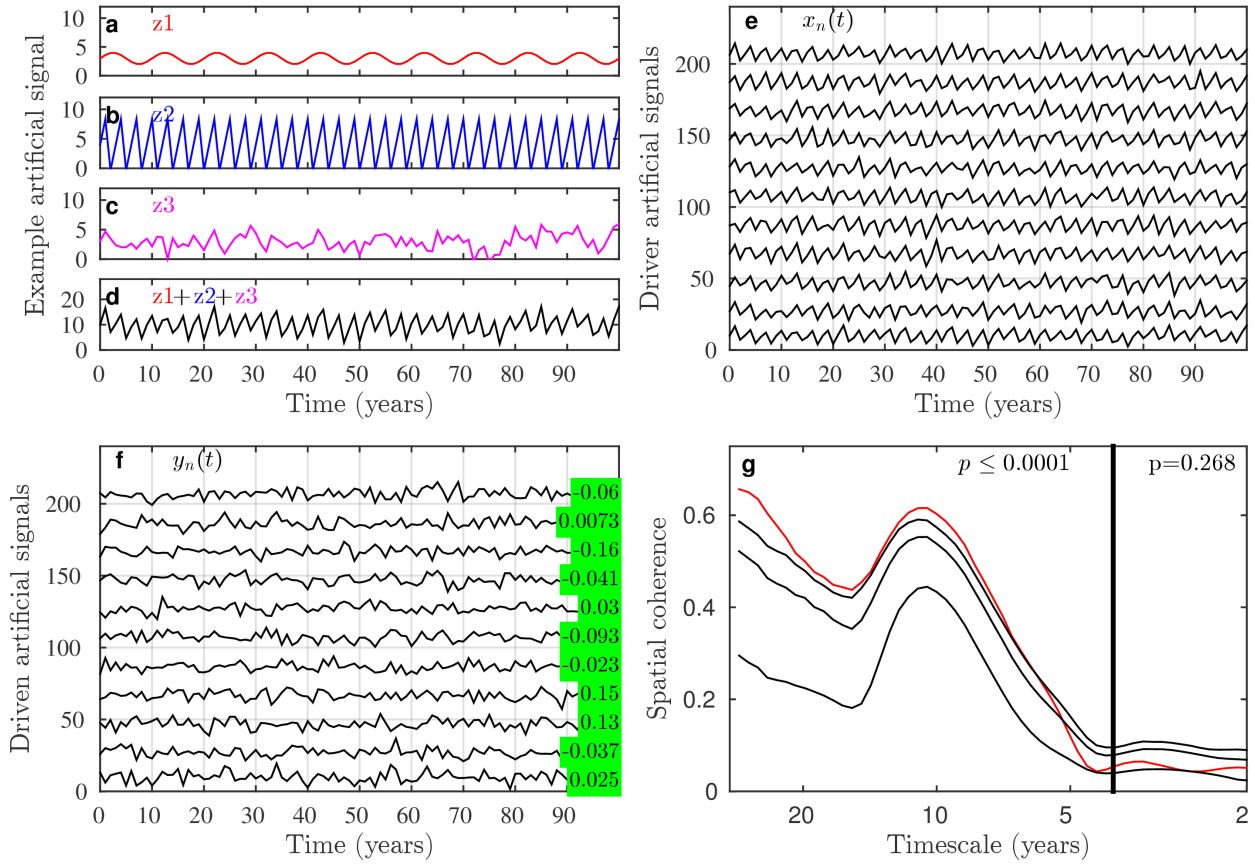

Supplementary Figure 5. Measuring relationships between variables using spatial coherence. The time series of panel e were used as drivers in producing the time series of panel f and the figure shows how this relationship can be detected with the spatial coherence technique. The time series of panel e were constructed as the sum of: 1) a single common signal of amplitude 1 and period 10 years (a); 2) a single common signal of amplitude 5 and period 3 years (b); and 3) white noise of standard deviation 1.5, independently generated for each of the 11 time series (c). The time series of panel f were produced via the relationship $y_n(t) = (\sum_{k=0}^{2} x_n(t-k))/3 + \epsilon_n(t)$ where the $\epsilon_n(t)$ were independent normal random numbers of mean 0 and standard deviation 3. This transmits the period-10 component of the x signals to the y but not the period-3 component because averaging covers a whole period for that component. Correlations (f, green numbers) between $x_n(t)$ and $y_n(t)$ did not indicate any particular relationship. Correlations cannot detect the relationship between the x and y because the technique confounds phenomena occurring on different timescales. Spatial coherences revealed a highly significant relationship at periods around 10 years (g) and on average over long timescales (left p-value on panel g, long timescales defined as > 4 years) but no relationship (right p-value) for short timescales (≤ 4 years). The red line on g is the spatial coherence and black lines are 50th, 95th, and 99th percentiles of spatial coherences of surrogate datasets appropriately representing the null hypothesis of no relationship between the x and y (see Methods).

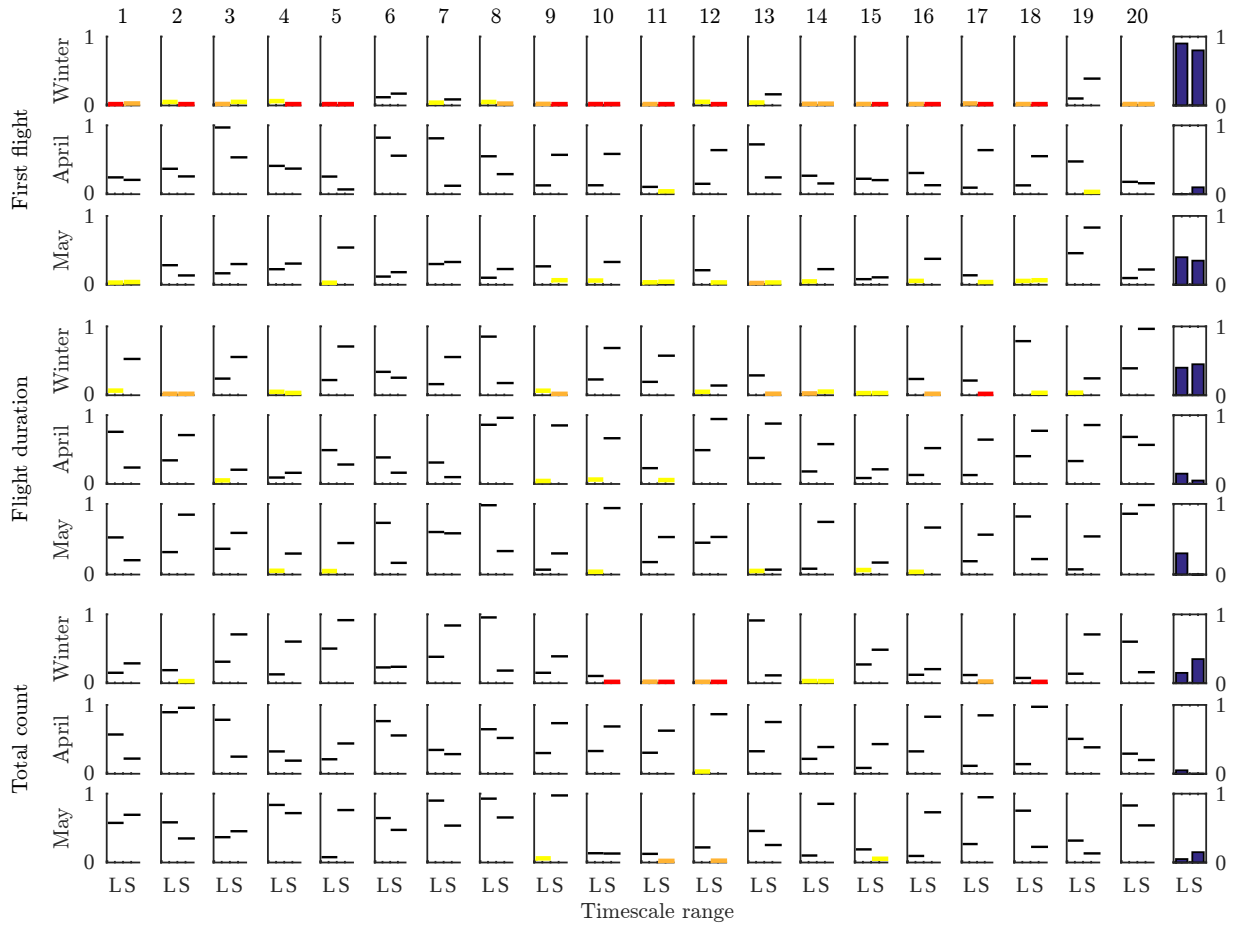

Supplementary Figure 6. Significances of spatial coherences between aphid and environmental variables. Bar heights and colours are p values for spatial coherences between aphid variables named in the outer left margin and average temperatures during the periods named in the inner left margin, for long (L) and short (S) timescales. Species codes and bar colours as in Fig. 1. First flight-winter temperature coherences are the same as in Fig. 1, and are presented again to facilitate comparisons. Blue bars at right are proportions of species significant at the 0.05 level. Significant spatial coherences that occurred between first flights and April or May temperatures were seldom more significant than coherences with winter temperature, and may have happened because April and May temperatures are themselves coherent with winter temperatures. We tested whether winter temperatures might have shown more significant coherences with first flights than April and May temperatures simply because winter temperatures are an average over a longer period and hence may be less intrinsically variable; this was not the case, as spatial coherences between temperatures for individual winter months and first flights were also much stronger than those between April or May temperatures and first flights.

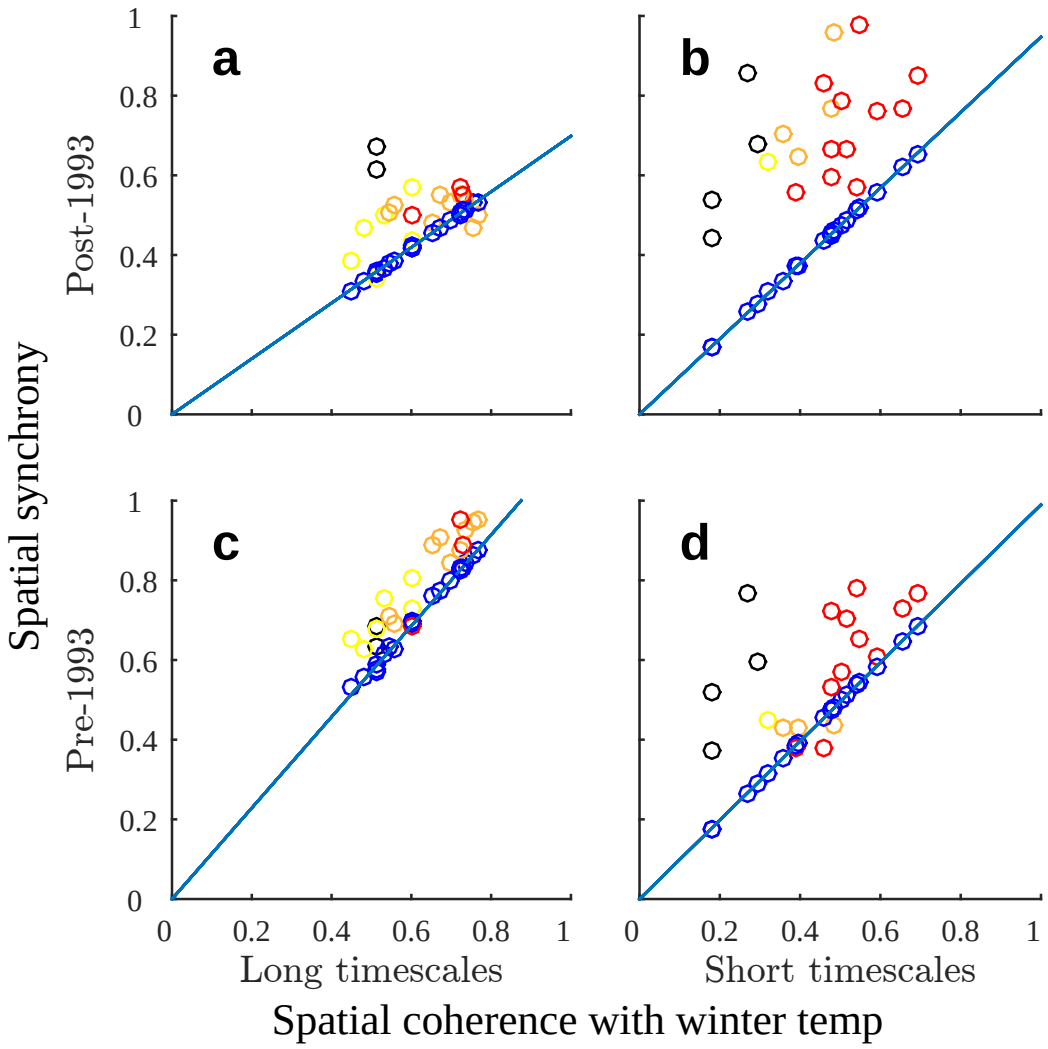

Supplementary Figure 7. Exact version of Fig. 2. Same as Fig. 2, but with blue points added as described in Supplementary notes, for the purpose described in Methods. These points show a more accurate value of the strength of synchrony (vertical axis value) predicted by the wavelet Moran theorem for the black, yellow, orange, and red points if winter temperature were the only synchronizing factor. The more accurate value is obtained by finding the prediction (coherence times environmental mean field) at each frequency and averaging over the frequency band, instead of plotting the product of average coherence and average mean field for the band (details in Supplementary notes). The difference is small.

2 Supplementary tables

Supplementary Table 1. Sampling sites used. Edinburgh is the combination of two very nearby sites, East Craigs and Gogarbank. East Craigs operating dates were 3/4/1969 to 2/10/1971 and 1/1/1972 to 30/12/2005. Gogarbank operating dates were 18/5/2004 to 13/12/2009. Data for Edinburgh were taken from 1/1/2006 forward from Gogarbank.

Site	Latitude	Longitude	Operation dates through 2010
Ayr	55.477	-4.567	30/8/1974 - 9/12/2001; 23/3/2003 - 25/12/2005
Broom's Barn	52.26	0.57	22/3/1965 - end
Dundee	56.457	-3.069	12/5/1965 - 10/12/2006; 17/2/2008 - 30/12/2008; 25/4/2010 - end
Edinburgh	55.949	-3.312	3/4/1969 - 2/10/1971; 1/1/1972 - 30/12/2005; 18/5/2004 - 13/12/2009
Hereford	52.125	-2.637	12/7/1971 - end
Newcastle	55.213	-1.682	21/5/1965 - end, excluding 2009
Preston	53.854	-2.763	29/4/1971 - end
Rothamsted	51.807	-0.356	29/4/1964 - end
Starcross	50.628	-3.454	5/2/1970 - 21/12/2008
Writtle	51.733	0.427	22/5/1975 - 29/7/1991; 1/1/1992 - end
Wye	51.185	0.939	30/11/1966 - end, excluding 2009

Supplementary Table 2. Species names.

ID	Common name	Latin binomial
1	Apple–grass aphid	*Rhopalosiphum insertum*
2	Bird cherry–oat aphid	*Rhopalosiphum padi*
3	Black bean aphid	*Aphis fabae*
4	Blackberry–cereal aphid	*Sitobion fragariae*
5	Blackcurrant–sowthistle aphid	*Hyperomyzus lactucae*
6	Corn leaf aphid	*Rhopalosiphum maidis*
7	Currant–lettuce aphid	*Nasonovia ribisnigri*
8	Damson–hop aphid	*Phorodon humuli*
9	Grain aphid	*Sitobion avenae*
10	Green spruce aphid	*Elatobium abietinum*
11	Leaf-curling plum aphid	*Brachycaudus helichrysi*
12	Mealy cabbage aphid	*Brevicoryne brassicae*
13	Mealy plum aphid	*Hyalopterus pruni*
14	Pea aphid	*Acyrthosiphon pisum*
15	Peach–potato aphid	*Myzus persicae*
16	Potato aphid	*Macrosiphum euphorbiae*
17	Rose–grain aphid	*Metopolophium dirhodum*
18	Shallot aphid	*Myzus ascalonicus*
19	Sycamore aphid	*Drepanosiphum platanoidis*
20	Willow–carrot aphid	*Cavariella aegopodii*

Supplementary Table 3. Locations of 13 long-running weather stations in the UK. Data were used from these stations (see Methods).

Location name	Latitude	Longitude
Armagh	54.352	-6.649
Bradford	53.813	-1.772
Durham	54.768	-1.585
Lerwick	60.139	-1.183
Lowestoft	52.483	1.727
Naim	57.593	-3.821
Oxford	51.761	-1.262
Ross on Wye	51.911	-2.584
Sheffield	53.381	-1.490
Stornoway	58.241	-6.318
Tiree	56.500	-6.880
Valley	53.252	-4.535
Wick Airport	58.454	-3.088

3 Supplementary equations

Lemma 1. *The mean squared magnitude of the wavelet mean field, $\frac{1}{T}\sum_{t=1}^{T}|r_\sigma(t)|^2$, satisfies*

$$\frac{1}{T}\sum_{t=1}^{T}|r_\sigma(t)|^2 = \frac{\frac{1}{T}\sum_{t=1}^{T}\left[\left(\frac{1}{N}\sum_{n=1}^{N}W_{n,\sigma}(t)\right)\left(\frac{1}{N}\sum_{n=1}^{N}\overline{W_{n,\sigma}(t)}\right)\right]}{\frac{1}{N}\sum_{n=1}^{N}\frac{1}{T}\sum_{t=1}^{T}W_{n,\sigma}(t)\overline{W_{n,\sigma}(t)}} \tag{1}$$

and

$$0 \leq \frac{1}{T}\sum_{t=1}^{T}|r_\sigma(t)|^2 \leq 1, \tag{2}$$

with

$$\frac{1}{T}\sum_{t=1}^{T}|r_\sigma(t)|^2 = 1 \tag{3}$$

if and only if all the time series are identical. The denominator of the right side of equation (1) *is the average of the powers of all the time series, $x_n(t)$, and the numerator is the power of the average time series, and hence equation* (1) *is a timescale-specific generalization of*

$$\frac{\mathrm{var}\left(\frac{1}{N}\sum_{n=1}^{N}x_n(t)\right)}{\left(\frac{1}{N}\sum_{n=1}^{N}\mathrm{var}(x_n(t))\right)}. \tag{4}$$

Proof. For brevity and clarity, we omit subscripts σ and time arguments t, sums over n and m are understood to be from 1 to N, and sums over t are understood to be from 1 to T. The mean field is

$$r = \frac{1}{N}\sum_n w_n = \frac{1}{N}\sum_n \frac{W_n}{\sqrt{\frac{1}{NT}\sum_n\sum_t W_n\overline{W_n}}}, \tag{5}$$

so the squared magnitude is

$$|r|^2 = \frac{\left(\frac{1}{N}\sum_n W_n\right)\left(\frac{1}{N}\sum_n \overline{W_n}\right)}{\frac{1}{NT}\sum_n\sum_t W_n\overline{W_n}}, \tag{6}$$

and the average over time is

$$\frac{1}{T}\sum_t |r|^2 = \frac{\frac{1}{T}\sum_t\left[\left(\frac{1}{N}\sum_n W_n\right)\left(\frac{1}{N}\sum_n \overline{W_n}\right)\right]}{\frac{1}{N}\sum_n\frac{1}{T}\sum_t W_n\overline{W_n}}, \tag{7}$$

proving the first part of the lemma. To prove $\frac{1}{T}\sum_t|r|^2 \leq 1$ with equality if and only if all time series are identical, let

$$P_n = \frac{1}{T}\sum_t |W_n|^2 \tag{8}$$

be the power of the nth transform, let

$$c(n,m) = \frac{\frac{1}{T}\sum_t |W_n||W_m|}{\sqrt{P_n}\sqrt{P_m}} \tag{9}$$

be a normalised inner product of the transform magnitudes at locations n and m, and consider the quantities

$$Q_1 = \frac{\frac{1}{N}\sum_n\frac{1}{N}\sum_m\frac{1}{T}\sum_t W_n\overline{W_m}}{\frac{1}{NT}\sum_n\sum_t|W_n|^2} = \frac{1}{T}\sum_t|r|^2, \tag{10}$$

$$Q_2 = \frac{\frac{1}{N}\sum_n\frac{1}{N}\sum_m c(n,m)\sqrt{P_n}\sqrt{P_m}}{\frac{1}{N}\sum_n P_n}, \tag{11}$$

and

$$Q_3 = \frac{(\frac{1}{N}\sum_n \sqrt{P_n})^2}{\frac{1}{N}\sum_n (\sqrt{P_n})^2}. \tag{12}$$

Q_1 is a real positive quantity made up of a sum of complex numbers $W_n\overline{W_m}$ and their complex conjugates, with a maximum when the phase difference between W_n and W_m is 0 at all times and for all n and m. Thus

$$Q_1 \leq \frac{\frac{1}{N}\sum_n \frac{1}{N}\sum_m \frac{1}{T}\sum_t |W_n||W_m|}{\frac{1}{NT}\sum_n \sum_t |W_n|^2}, \tag{13}$$

with equality if and only if phase synchronization of the time series is perfect. But the right side of equation (13) is Q_2. Because $0 \leq c(n,m) \leq 1$, Q_2 is, in turn, maximized when the $c(n,m)$ are all 1, so

$$Q_2 \leq \frac{\frac{1}{N}\sum_n \frac{1}{N}\sum_m \sqrt{P_n}\sqrt{P_m}}{\frac{1}{N}\sum_n P_n}. \tag{14}$$

The maximum is the value of Q_2 if and only if the varying transform magnitudes at all sites have correlation coefficient 1 (i.e., all the $c(n,m)$ are 1). But the right side of equation (14) is Q_3. And the mean square of a set of real numbers is always greater than or equal to the squared mean (because the function $f(x) = x^2$ is concave upward), so

$$Q_3 \leq 1, \tag{15}$$

with equality if and only if all the P_n are the same. So

$$\frac{1}{T}\sum_t |r|^2 = Q_1 \leq Q_2 \leq Q_3 \leq 1, \tag{16}$$

with the first and last terms being equal if and only if phase synchronization of the time series is perfect, the time-varying magnitudes of all transforms are perfectly correlated, and the powers of all time series are the same - in other words if and only if all the time series are identical. □

Lemma 2. *The spatial coherence,* $|\Pi_\sigma^{(01)}|$*, is between* 0 *and* 1.

Proof. We again omit subscripts σ and time arguments t, sums over n are understood to be from 1 to N, and sums over t are understood to be from 1 to T.

$$\Pi^{(01)} = \frac{1}{NT}\sum_n \sum_t w_n^{(b)}\overline{w_n^{(e)}} \tag{17}$$

$$= \frac{\frac{1}{NT}\sum_n \sum_t W_n^{(b)}\overline{W_n^{(e)}}}{\sqrt{\frac{1}{NT}\sum_n \sum_t W_n^{(b)}\overline{W_n^{(b)}}}\sqrt{\frac{1}{NT}\sum_n \sum_t W_n^{(e)}\overline{W_n^{(e)}}}} \tag{18}$$

$$= \frac{\sum_n \sum_t W_n^{(b)}\overline{W_n^{(e)}}}{\sqrt{\sum_n \sum_t W_n^{(b)}\overline{W_n^{(b)}}}\sqrt{\sum_n \sum_t W_n^{(e)}\overline{W_n^{(e)}}}} \tag{19}$$

Therefore the spatial coherence is

$$|\Pi^{(01)}| = \frac{\left|\sum_n \sum_t W_n^{(b)}\overline{W_n^{(e)}}\right|}{\sqrt{\sum_n \sum_t W_n^{(b)}\overline{W_n^{(b)}}}\sqrt{\sum_n \sum_t W_n^{(e)}\overline{W_n^{(e)}}}}, \tag{20}$$

which is less than or equal to 1 by the Cauchy-Schwarz inequality. Cauchy-Schwarz also tells us that equality happens if and only if there is a complex number α (which can depend on σ) such that $\alpha W_n^{(b)} = W_n^{(e)}$. □

For the following theorem, we observe that for given σ, the normalized wavelet components $w_{n,\sigma}^{(b)}(t)$ and $w_{n,\sigma}^{(e)}(t)$ can be viewed as points in the complex space $\mathbb{C}^D$, where D is the product of N and the number of time steps, t, for which $w_{n,\sigma}^{(b)}(t)$ and $w_{n,\sigma}^{(e)}(t)$ are defined. We use the inner product $w_{n,\sigma}^{(b)}(t) \cdot w_{n,\sigma}^{(e)}(t) = \frac{1}{NT}\sum_n \sum_t w_{n,\sigma}^{(b)}(t)\overline{w_{n,\sigma}^{(e)}(t)}$ on the space, and denote the associated norm by $\|\cdot\|$.

Theorem 3. The wavelet Moran theorem. *We can write* $w^{(b)}_{n,\sigma}(t) = \Pi^{(be)}_\sigma w^{(e)}_{n,\sigma}(t) + d_{n,\sigma}(t)$*, where this equation defines* $d_{n,\sigma}(t)$*. Then* $w^{(e)}_{n,\sigma}(t) \cdot d_{n,\sigma}(t) = 0$ *and for each* σ*,* $\Pi^{(be)}_\sigma$ *is the complex value that minimizes* $\|d_{n,\sigma}(t)\|$*. The* $d_{n,\sigma}(t)$ *can be interpreted as residuals. The time average of the squared magnitude of the mean field of the biological transforms is*

$$\begin{aligned}
\frac{1}{T}\sum_{t=1}^{T} |r^{(b)}_\sigma(t)|^2 &= |\Pi^{(be)}_\sigma|^2 \frac{1}{T}\sum_{t=1}^{T} |r^{(e)}_\sigma(t)|^2 && (21)\\
&+ \frac{1}{TN^2}\sum_{t=1}^{T}\sum_{n=1}^{N}\sum_{m\neq n} 2\,\mathrm{Re}(\Pi^{(be)}_\sigma w^{(e)}_{n,\sigma}(t)\overline{d_{m,\sigma}(t)}) && (22)\\
&+ \frac{1}{T}\sum_{t=1}^{T}\left|\frac{1}{N}\sum_{n=1}^{N} d_{n,\sigma}(t)\right|^2. && (23)
\end{aligned}$$

If populations do not interact with populations at neighbouring sites, nor are they directly affected by environments in neighbouring sites, interpreted as the term in (22) *being negligible (see justification in the proof below), then*

$$\frac{1}{T}\sum_{t=1}^{T} |r^{(b)}_\sigma(t)|^2 \approx |\Pi^{(be)}_\sigma|^2 \frac{1}{T}\sum_{t=1}^{T} |r^{(e)}_\sigma(t)|^2 + \frac{1}{T}\sum_{t=1}^{T}\left|\frac{1}{N}\sum_{n=1}^{N} d_{n,\sigma}(t)\right|^2. \quad (24)$$

In other words, synchrony of the ecological variable can be divided into a component due to variable e and residual synchrony. It follows that $\left\langle |r^{(b)}_\sigma(t)|\right\rangle \geq |\Pi^{(be)}_\sigma| \left\langle |r^{(e)}_\sigma(t)|\right\rangle$*. If, in addition, the only synchronizing influence on the populations is variable e, interpreted as the second term on the right side of equation* (24) *being negligible, then*

$$\frac{1}{T}\sum_{t=1}^{T} |r^{(b)}_\sigma(t)|^2 \approx |\Pi^{(be)}_\sigma|^2 \frac{1}{T}\sum_{t=1}^{T} |r^{(e)}_\sigma(t)|^2 \quad (25)$$

and $\left\langle |r^{(b)}_\sigma(t)|\right\rangle \approx |\Pi^{(be)}_\sigma| \left\langle |r^{(e)}_\sigma(t)|\right\rangle$*. Thus* $|\Pi^{(be)}_\sigma| \left\langle |r^{(e)}_\sigma(t)|\right\rangle$ *gives the amount of synchrony explained solely by the synchronizing influence of variable e.*

Proof. As previously, we omit subscripts σ and time arguments t, sums over n and m are understood to be from 1 to N, and sums over t are understood to be from 1 to T. The decomposition $w^{(b)}_n = \Pi^{(be)} w^{(e)}_n + d_n$, as well as $w^{(e)}_n \cdot d_n = 0$ and the minimality of $\|d_n\|$, follow from standard theory of inner product spaces. We then compute

$$\begin{aligned}
|r^{(b)}|^2 &= \left(\frac{1}{N}\sum_n w^{(b)}_n\right)\left(\frac{1}{N}\sum_m \overline{w^{(b)}_m}\right) && (26)\\
&= \frac{1}{N^2}\left(\sum_n (\Pi^{(be)} w^{(e)}_n + d_n)\right)\left(\sum_m (\overline{\Pi^{(be)}}\,\overline{w^{(e)}_m} + \overline{d_m})\right)\\
&= \frac{1}{N^2}\sum_n\sum_m \left(\Pi^{(be)} w^{(e)}_n \overline{\Pi^{(be)}}\,\overline{w^{(e)}_m} + d_n \overline{\Pi^{(be)}}\,\overline{w^{(e)}_m} + \Pi^{(be)} w^{(e)}_n \overline{d_m} + d_n \overline{d_m}\right)\\
&= |\Pi^{(be)}|^2 |r^{(e)}|^2 + \frac{1}{N^2}\sum_n\sum_m 2\,\mathrm{Re}(\Pi^{(be)} w^{(e)}_n \overline{d_m}) + \left|\frac{1}{N}\sum_n d_n\right|^2. && (27)
\end{aligned}$$

Taking the time average and using the fact that the residuals, d_n, are orthogonal to the $w^{(e)}_n$ to exclude summands with $m = n$ in the middle term of (27),

$$\frac{1}{T}\sum_t |r^{(b)}|^2 = |\Pi^{(be)}|^2 \frac{1}{T}\sum_t |r^{(e)}|^2 + \frac{1}{TN^2}\sum_t\sum_n\sum_{m\neq n} 2\,\mathrm{Re}(\Pi^{(be)} w^{(e)}_n \overline{d_m}) + \frac{1}{T}\sum_t \left|\frac{1}{N}\sum_n d_n\right|^2, \quad (28)$$

which is the same as equation (21) - (23). The remaining claims follow straightforwardly.

The assumption of non-interacting populations not directly affected by the environments of neighbouring sites was interpreted to mean (22) is negligible. This is reasonable because, for such populations, the magnitude of $\frac{1}{TN^2}\sum_t\sum_n\sum_{m\neq n} w_n^{(e)}\overline{d_m}$ should be negligible, as it quantifies relationships between environmental fluctuations at site n, measured with $w_n^{(e)}$, and residuals at other sites, d_m. In particular, (22) is exactly 0 when the environment is perfectly synchronized as measured by the $w_n^{(e)}$, i.e., all the $w_n^{(e)}$ are the same. Environmental drivers are often very highly synchronized on large spatial scales, as for the winter temperature data analysed in this study. We tested the assumption that the cross terms in (22) are negligible for aphid first flight and winter temperature, finding that they were (Supplementary notes).

□

4 Supplementary notes

We tested whether the cross terms in the wavelet Moran theorem, i.e. the terms (22), were indeed negligible for first-flight and winter temperature, as expected if populations do not interact with populations at neighbouring sites nor are they directly affected by environments in neighbouring sites. The quantity

$$\frac{\frac{1}{TN^2}\sum_{t=1}^{T}\sum_{n=1}^{N}\sum_{m\neq n} 2\,\mathrm{Re}(\Pi_\sigma^{(be)} w_{n,\sigma}^{(e)}(t)\overline{d_{m,\sigma}(t)})}{\frac{1}{T}\sum_{t=1}^{T}|r_\sigma^{(b)}(t)|^2} \tag{29}$$

was averaged over low (respectively, high) frequencies for each species, and resulting values were averaged across species. The result was 6.44% (respectively, 4.27%), supporting the decision to neglect the terms.

The wavelet Moran theorem provides the expectation that if the environmental driver e is the only synchronizing influence, then

$$\sqrt{\frac{1}{T_{\mathrm{half}}}\sum_{t=t_i}^{t_f}|r_\sigma^{(b)}(t)|^2} \approx |\Pi_\sigma^{(be)}|\sqrt{\frac{1}{T_{\mathrm{half}}}\sum_{t=t_i}^{t_f}|r_\sigma^{(e)}(t)|^2}, \tag{30}$$

where $T_{\mathrm{half}} = 17$ and t_i and t_f are initial and final times for either the early or late periods ($t_i = 1$ for 1976 and $t_f = 17$ for 1992 for the early period, or $t_i = 19$ for 1994 and $t_f = 35$ for 2010 for the late period). Averaging over frequencies,

$$\mathrm{mean}_{f\in F}\left(\sqrt{\frac{1}{T_{\mathrm{half}}}\sum_{t=t_i}^{t_f}|r_\sigma^{(b)}(t)|^2}\right) \approx \mathrm{mean}_{f\in F}\left(|\Pi_\sigma^{(be)}|\sqrt{\frac{1}{T_{\mathrm{half}}}\sum_{t=t_i}^{t_f}|r_\sigma^{(e)}(t)|^2}\right), \tag{31}$$

where F is either low or high frequencies. For conceptual clarity, the diagonal lines in Fig. 2 were instead based on

$$\mathrm{mean}_{f\in F}\left(\sqrt{\frac{1}{T_{\mathrm{half}}}\sum_{t=t_i}^{t_f}|r_\sigma^{(b)}(t)|^2}\right) \approx \mathrm{mean}_{f\in F}\left(|\Pi_\sigma^{(be)}|\right)\mathrm{mean}_{f\in F}\left(\sqrt{\frac{1}{T_{\mathrm{half}}}\sum_{t=t_i}^{t_f}|r_\sigma^{(e)}(t)|^2}\right); \tag{32}$$

the left side and the first multiplicand on the right are the vertical and horizontal axis quantities on Fig. 2, respectively, and the second multiplicand gives the Fig. 2 diagonal line slopes. The approximation

$$\mathrm{mean}_{f\in F}\left(|\Pi_\sigma^{(be)}|\sqrt{\frac{1}{T_{\mathrm{half}}}\sum_{t=t_i}^{t_f}|r_\sigma^{(e)}(t)|^2}\right) \approx \mathrm{mean}_{f\in F}\left(|\Pi_\sigma^{(be)}|\right)\mathrm{mean}_{f\in F}\left(\sqrt{\frac{1}{T_{\mathrm{half}}}\sum_{t=t_i}^{t_f}|r_\sigma^{(e)}(t)|^2}\right) \tag{33}$$

is reasonable if either one or the other of the multiplicands inside the mean on the left does not vary too much in the frequency band F. To test this approximation, we produced a version of Fig. 2 augmented by the points

$$\left(\mathrm{mean}_{f\in F}\left(|\Pi_\sigma^{(be)}|\right), \mathrm{mean}_{f\in F}\left(|\Pi_\sigma^{(be)}|\sqrt{\frac{1}{T_{\mathrm{half}}}\sum_{t=t_i}^{t_f}|r_\sigma^{(e)}(t)|^2}\right)\right). \tag{34}$$

The points indicate expectations of the wavelet Moran theorem without relying on the approximation. It looked virtually the same as Fig. 2 (Supplementary Fig. 7).